Vertical Differencing of the Primitive Equations Based on the Charney–Phillips Grid in Hybrid σ–p Vertical Coordinates

AKIO ARAKAWA AND CELAL S. KONOR

Department of Atmospheric Sciences, University of California, Los Angeles, Los Angeles, California

(Manuscript received 1 May 1995, in final form 6 September 1995)

ABSTRACT

Two types of vertical grids are used for atmospheric models: the Lorenz grid (L grid) and the Charney–Phillips grid (CP grid). Although the CP grid is the standard grid for quasigeostrophic models, it is not widely used in the primitive equation models because it is easier with the L grid to maintain some of the integral properties of the continuous system.

In this paper, problems with the L grid are pointed out that are due to the existence of an extra degree of freedom in the vertical distribution of the temperature (and the potential temperature). Then a vertical differencing of the primitive equations based on the CP grid is presented, while most of the advantages of the L grid in a hybrid σ–p vertical coordinate are maintained. The discrete hydrostatic equation is constructed in such a way that it is free from the vertical computational mode in the thermal field. Also, the vertical advection of the potential temperature in the discrete thermodynamic equation is constructed in such a way that it reduces to the standard (and most straightforward) vertical differencing of the quasigeostrophic equations based on the CP grid.

Simulations of standing oscillations superposed on a resting atmosphere are presented using two vertically discrete models, one based on the L grid and the other on the CP grid. The comparison of the simulations shows that with the L grid a stationary vertically zigzag pattern dominates in the thermal field, while with the CP grid no such pattern is evident. Simulations of the growth of an extratropical cyclone in a cyclic channel on a β plane are also presented using two different σ-coordinate models, again one with the L grid and the other with the CP grid, starting from random disturbances. The L grid simulation is dominated by short waves, while there is no evidence of short-wave growth in the CP grid simulation.

1. Introduction

Vertical discretization of the governing equations remains one of the most basic problems in constructing a three-dimensional numerical model of the atmosphere. Since the atmosphere is highly inhomogeneous in the vertical, the problem of vertical discretization is generally less straightforward than that of horizontal discretization.

Charney and Phillips (1953) constructed a discrete three-dimensional quasigeostrophic model based on the pressure coordinate. The sigma-coordinate version of the vertical grid they used, which we referred to as the Charney–Phillips grid or CP grid, is shown in Fig. 1b. In this grid, potential temperatures are carried at the levels carrying vertical mass fluxes, which are in-between the levels carrying horizontal velocities (and, therefore, geopotentials). Thus, the thickness between two adjacent velocity levels can be made depending solely on the potential temperature at the level in between, and the vertical advection of the potential temperature in the thermodynamic equation depending solely on the vertical mass flux at that level to which the equation is applied.

Quasigeostrophic motion is governed by conservation of the quasigeostrophic (pseudo) potential vorticity during horizontal advection by the geostrophic velocity. It can be shown that the vertical differencing used by Charney and Phillips (1953), which is the most straightforward vertical differencing for the CP grid, maintains conservation of the quasigeostrophic (pseudo) potential vorticity during the advection processes (see Arakawa and Moorthi 1988).

Lorenz (1960), on the other hand, constructed a vertically discrete balanced model, which conserves the total energy, the mean potential temperature, and the variance of the potential temperature under adiabatic (and frictionless) processes. For this purpose, he deviated from the CP grid by introducing a new grid. The sigma-coordinate version of that grid, which we referred to the Lorenz grid or L grid, is shown in Fig. 1a. Unlike the CP grid, the L grid carries horizontal velocities and potential temperatures at the same levels that represent model layers, while vertical mass fluxes are carried at the interfaces of such layers. With this dis-

Corresponding author address: Dr. Akio Arakawa, Department of Atmospheric Science, University of California, Los Angeles, 405 Hilgard Avenue, Los Angeles, CA 90024-1565.

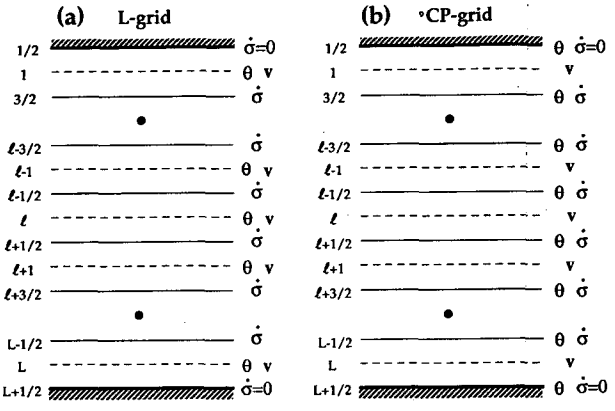

FIG. 1. An illustration of (a) the Lorenz grid and (b) the Charney–Phillips grid for a σ coordinate.

tribution of the variables, it is more straightforward to keep track of the budgets of the quantities to be predicted, and thus it is easier to maintain conservation properties mentioned above.

Following Lorenz's approach for the balanced model, Arakawa and Lamb (1977) constructed a vertically discrete primitive equation model that maintains four integral constraints on the continuous system of equations (see section 2b). The first two of these constraints, which are presumably more important than the other two when the sigma coordinate is used, are also satisfied by the vertical discretizations by Simmons and Burridge (1981) and Arakawa and Suarez (1983).

Some problems, however, have been recognized with the L grid. One of them is the existence of a computational mode in the vertical distribution of the potential temperature (Tokioka 1978; Arakawa 1988; Cullen and James 1994; Hollingsworth 1995). It is caused by the fact that, with a centered or approximately centered finite differencing, the thickness between two adjacent layers depends on an average of the potential temperatures of the two layers. Figure 2 demonstrates this situation. Let us assume that Φ' and θ' are the deviations of the geopotential and potential temperature from a reference state, respectively. It is possible to have a zero vertical distribution of Φ' for a nonzero vertical distribution of θ' since θ' of the two adjacent layers is averaged to obtain the vertical difference of Φ' from the discrete hydrostatic equation. The zigzag vertical structure of the potential temperature, therefore, can be completely decoupled from the dynamics of the discrete system.

More generally, we may say that in an N-layer model based on the L grid, there are N degrees of freedom in the vertical distribution of potential temperature, while there are only $N - 1$ degrees of freedom in the vertical distribution of vertical mass flux. This means that there is an extra degree of freedom in the vertical distribution of potential temperature that cannot be controlled by any internal modes. Thus, this problem with the L grid is a property of the vertical grid rather than a particular vertical-difference scheme. It is clear that the computational mode does not exist in a model with the CP grid.

The problem of the existence of the computational mode can be serious, especially in the models that include moist processes, since the computational mode can spuriously interact with the physical mode through inherently nonlinear condensation and associated processes. An example of the latter is the effect of cloud layers generated by the zigzag vertical structure of the potential temperature on the radiation field.

Another difficulty with the L grid is the spurious amplification of short waves due to baroclinic instability (Arakawa and Moorthi 1988). This occurs due to a false satisfaction of the necessary condition for baroclinic instability due to an excess degree of freedom in the vertical distribution of the potential vorticity. Arakawa and Moorthi (1988) showed that this problem does not exist in a model based on the CP grid at least when $\beta = 0$.

Despite its disadvantages mentioned above, majority of the existing primitive equation models are based on the L grid (e.g., Bourke 1974; Arakawa and Lamb 1977; Simmons and Burridge 1981; Arakawa and Suarez 1983), and the CP grid has not been commonly used in the primitive equation models. Notable exceptions are models developed by Krishnamurti (1969) and Robert et al. (1972). Neither of these models, however, explicitly consider the problem of maintaining integral constraints on the continuous system.

The purpose of this paper is to present a vertical discretization of the primitive equations that satisfies most of the integral constraints suggested by Arakawa and Lamb (1977) using the CP grid in a generalized σ coordinate, $\sigma \equiv F(p, p_S)$. Some examples showing the performance of the discrete model are also shown.

In a vertically discrete system based on a σ coordinate, the errors due to discretization of the pressure gradient force can be serious near steep surface topog-

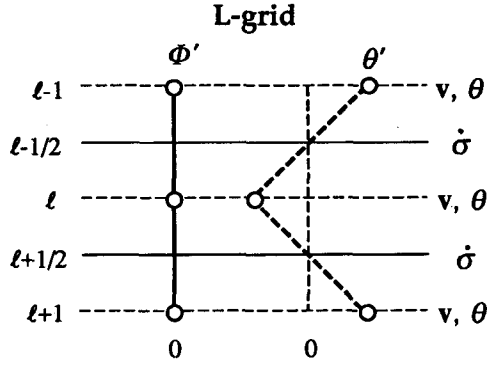

FIG. 2. An illustration of the computational mode on a portion of the L grid.

raphy. To reduce systematic effects of these errors, Arakawa and Lamb (1977) constrain the vertically integrated discrete pressure gradient force to generate no circulation along a contour of surface topography. Here we also use this constraint in constructing the discrete pressure gradient force with the CP grid. In addition, to reduce the errors away from the surface, we allow the possibility of using the generalized σ coordinate, in which the coordinate can gradually become independent from the surface pressure with height, as in Simmons and Burridge (1981).

Section 2 reviews the basic governing equations in a generalized σ coordinate and some of their integral properties for the continuous case. In section 3, we derive the vertically discrete equations, which satisfy two of the four integral constraints used by Arakawa and Lamb (1977). In section 4, we present numerical simulations of standing gravity waves using two models, one based on the L grid and the other on the CP grid, to demonstrate the difference between the two models in view of the computational mode. Section 4 presents numerical simulations of nonlinear evolution of an extratropical cyclone by using two models, again one based on the L grid and the other on the CP grid. The results of similar simulations with a diffusion term in the thermodynamic equation with different magnitudes of coefficients are also shown in section 4. Finally, conclusions and a summary of the discrete model equations presented in this paper are given in section 5.

2. Basic governing equations

a. *Equations in a generalized σ coordinate*

In this section we present basic governing equations using a generalized σ coordinate defined by

$$\sigma \equiv F(p, p_S), \tag{2.1}$$

where p is the pressure and p_S is the surface pressure. It is assumed that $\sigma \equiv F(p, p_S)$ monotonically decreases with height. When $F(p, p_S) \equiv p/p_S$, the coordinate reduces to the original σ coordinate proposed by Phillips (1957). When $F(p, p_S) \equiv p/p_S + (p/p_S - 1)(p/p_S - p/p_C)$, on the other hand, where p_C is a constant, it reduces to the coordinate used by Simmons and Burridge (1981).

With the σ coordinate, the material time derivative is expressed as

$$\frac{D}{Dt} \equiv \left(\frac{\partial}{\partial t}\right)_\sigma + \mathbf{v}\cdot\nabla_\sigma + \dot{\sigma}\frac{\partial}{\partial \sigma}, \tag{2.2}$$

where $\mathbf{v}$ is the horizontal velocity and $\dot{\sigma} \equiv D\sigma/Dt$. The vertical p-velocity ω, for example, can be expressed as

$$\omega \equiv \frac{Dp}{Dt} = \left(\frac{\partial p}{\partial t}\right)_\sigma + \mathbf{v}\cdot\nabla_\sigma p + m\dot{\sigma}, \tag{2.3}$$

where

$$m \equiv \frac{\partial p}{\partial \sigma}. \tag{2.4}$$

When divided by the gravitational acceleration g, m is the mass per unit increment of σ per unit horizontal area.

Using m, the hydrostatic equation can be written as

$$\frac{\partial \Phi}{\partial \sigma} = -\alpha m, \tag{2.5}$$

where Φ is the geopotential height and α is the specific volume. Also using m, we can write the continuity equation as

$$\left(\frac{\partial m}{\partial t}\right)_\sigma + \nabla_\sigma\cdot(m\mathbf{v}) + \frac{\partial}{\partial \sigma}(m\dot{\sigma}) = 0. \tag{2.6}$$

If the boundaries in the vertical are material surfaces, we have

$$(m\dot{\sigma}) = 0 \quad \text{at} \quad \sigma = \sigma_T, \sigma_S, \tag{2.7}$$

where the subscript T and S denote the upper and lower boundaries, respectively. We assume σ_T and σ_S are constants so that the boundaries are coordinate surfaces.

The model atmosphere is assumed to be a perfect gas, so that the equation of state is

$$\alpha = \frac{RT}{p}, \tag{2.8}$$

where R is the gas constant and T is the temperature. The potential temperature θ is given by

$$\theta = \frac{c_p T}{\Pi}, \tag{2.9}$$

where c_p is the specific heat at constant pressure and Π is the Exner function defined by

$$\Pi \equiv c_p\left(\frac{p}{p_0}\right)^\kappa, \tag{2.10}$$

p_0 is a reference pressure, and $\kappa \equiv R/c_p$. The thermodynamic equation is given by

$$c_p\frac{DT}{Dt} = c_p\left[\left(\frac{\partial T}{\partial t}\right)_\sigma + \mathbf{v}\cdot\nabla T + \dot{\sigma}\frac{\partial T}{\partial \sigma}\right] = \alpha\omega + Q, \tag{2.11}$$

where Q is the heating per unit mass. Using the potential temperature θ, the thermodynamic equation can also be written as

$$\frac{D\theta}{Dt} = \left(\frac{\partial \theta}{\partial t}\right)_\sigma + \mathbf{v}\cdot\nabla_\sigma\theta + \dot{\sigma}\frac{\partial \theta}{\partial \sigma} = \frac{Q}{\Pi}. \tag{2.12}$$

The momentum equation can be written as

$$\frac{D\mathbf{v}}{Dt} = \left(\frac{\partial \mathbf{v}}{\partial t}\right)_\sigma + \mathbf{v}\cdot\nabla_\sigma\mathbf{v} + \dot{\sigma}\frac{\partial \mathbf{v}}{\partial \sigma} = -(\nabla_p\Phi) - f\mathbf{k}\times\mathbf{v} + \mathbf{F}, \quad (2.13)$$

where $f \equiv 2\Omega \sin\varphi$ is the Coriolis parameter, Ω is earth's angular velocity, φ is the latitude, $\mathbf{k}$ is the vertical unit vector, and $\mathbf{F}$ is the friction force. Using the relation

$$\nabla_p = \nabla_\sigma - \nabla_\sigma p\frac{\partial}{\partial p} \quad (2.14)$$

and (2.4), the horizontal pressure gradient force can be written as

$$-\nabla_p\Phi = -\nabla_\sigma\Phi + \frac{1}{m}\frac{\partial\Phi}{\partial\sigma}\nabla_\sigma p. \quad (2.15)$$

Substituting (2.4) into the first term in (2.6), integrating with respect to σ from σ_T to σ, and using (2.7), we obtain the pressure tendency equation

$$\left(\frac{\partial p}{\partial t}\right)_\sigma = -\int_{\sigma_T}^{\sigma}\nabla_\sigma\cdot(m\mathbf{v})d\sigma - (m\dot{\sigma})_\sigma. \quad (2.16)$$

In deriving (2.16), p_T = const has been assumed. Applying (2.16) to $\sigma = \sigma_S$ and using (2.7), we obtain the surface pressure tendency equation

$$\frac{\partial p_S}{\partial t} = -\int_{\sigma_T}^{\sigma_S}\nabla_\sigma\cdot(m\mathbf{v})d\sigma. \quad (2.17)$$

Finally, we derive a diagnostic relationship to determine the vertical mass flux $m\dot{\sigma}$ by differentiating (2.1) with respect to time t under constant σ,

$$\left(\frac{\partial F}{\partial p}\right)_{p_S}\left(\frac{\partial p}{\partial t}\right)_\sigma + \left(\frac{\partial F}{\partial p_S}\right)_p\frac{\partial p_S}{\partial t} = 0, \quad (2.18)$$

and substituting (2.16) and (2.17) into (2.18) as

$$-\left(\frac{\partial F}{\partial p}\right)_{p_S}(m\dot{\sigma})_\sigma = \left(\frac{\partial F}{\partial p}\right)_{p_S}\int_{\sigma_T}^{\sigma}\nabla_\sigma\cdot(m\mathbf{v})d\sigma + \left(\frac{\partial F}{\partial p_S}\right)_p\int_{\sigma_T}^{\sigma_S}\nabla_\sigma\cdot(m\mathbf{v})d\sigma. \quad (2.19)$$

When $F \equiv p$, for which $m = 1$ and $\dot{\sigma} = \omega$, the vertical mass flux equation (2.19) gives

$$\omega = -\int_{p_T}^{p}\nabla_p\cdot\mathbf{v}dp, \quad (2.20)$$

which can be readily obtained from $\nabla_p\cdot\mathbf{v} + \partial\omega/\partial p = 0$ for the pressure coordinate. When $F \equiv (p - p_T)(p_S - p_T)^{-1}$ in (2.1), on the other hand, (2.19) becomes

$$-(m\dot{\sigma})_\sigma = \int_{\sigma_T}^{\sigma}\nabla_\sigma\cdot(m\mathbf{v})d\sigma - \sigma\int_{\sigma_T}^{\sigma_S}\nabla_\sigma\cdot(m\mathbf{v})d\sigma, \quad (2.21)$$

where $m = p_S - p_T$.

b. *Expressing integral constraints with the generalized σ coordinate*

In this section, we express a set of integral constraints using the generalized σ coordinate. These constraints, which were used by Arakawa and Lamb (1977) in designing a vertical difference scheme, are that (i) vertically integrated pressure gradient force generates no circulation along a contour of the surface topography; (ii) the energy conversion terms in the thermodynamic and kinetic energy equations have the same form with opposite signs so that the total energy is conserved under adiabatic frictionless processes; (iii) the global mass integral of the potential temperature is conserved under adiabatic processes; (iv) the global mass integral of a function of the potential temperature, such as a square or logarithm of the potential temperature, is also conserved under adiabatic processes.

1) VERTICALLY INTEGRATED HORIZONTAL PRESSURE FORCE

The horizontal pressure gradient force (2.15) can be rewritten as

$$-(\nabla_p\Phi) = -\frac{1}{m}\nabla_\sigma(m\Phi) + \frac{1}{m}\frac{\partial}{\partial\sigma}(\Phi\nabla_\sigma p). \quad (2.22)$$

Here (2.4) has been used. The vertical mass integral of (2.22) is

$$-\int_{\sigma_T}^{\sigma_S}m(\nabla_p\Phi)d\sigma = -\nabla_\sigma\int_{\sigma_T}^{\sigma_S}(m\Phi)d\sigma + \Phi_S\nabla_\sigma p_S. \quad (2.23)$$

When (2.23) is integrated along a contour of the surface of topography, on which Φ_S is constant, the right-hand side vanishes so that constraint (i) is satisfied.

2) CONSERVATION OF THE TOTAL ENERGY

Using (2.6) and (2.11), the thermodynamic energy equation can be written as

$$\left(\frac{\partial}{\partial t}\right)_\sigma(mc_pT) + \nabla_\sigma\cdot(mc_pT\mathbf{v}) + \frac{\partial}{\partial\sigma}(mc_pT\dot{\sigma}) = m(\alpha\omega + Q). \quad (2.24)$$

On the other hand, multiplying the momentum equation (2.13) with (2.15) by $m\mathbf{v}$ and using (2.3), (2.4), (2.5),

(2.6), and (2.22), we obtain the kinetic energy equation

$$\left(\frac{\partial}{\partial t}\right)_\sigma\left(m\frac{\mathbf{v}^2}{2}\right)+\nabla_\sigma\cdot\left(m\frac{\mathbf{v}^2}{2}\mathbf{v}\right)+\frac{\partial}{\partial\sigma}\left(m\frac{\mathbf{v}^2}{2}\dot{\sigma}\right)$$
$$=-\nabla_\sigma\cdot(m\Phi\mathbf{v})-\frac{\partial}{\partial\sigma}\left[\Phi\left(\frac{\partial p}{\partial t}+m\dot{\sigma}\right)\right]$$
$$-m\alpha\omega+m\mathbf{v}\cdot\mathbf{F}. \quad (2.25)$$

The first and second terms on the right-hand side of (2.25) represent convergence of horizontal and vertical energy fluxes that involve Φ. The term $m\alpha\omega$, on the other hand, represents the energy conversion from the total potential energy to kinetic energy. When the sum of (2.24), (2.25), and $\partial(\Phi_S p_S)/\partial t = \Phi_S(\partial p_S/\partial t)$ is integrated over the entire atmosphere, all terms vanish under adiabatic frictionless processes so that constraint (ii) is satisfied.

3) Conservation of the mass integrals of the potential temperature and its function under adiabatic processes

Using (2.6), the thermodynamic equation (2.12) can be rewritten as

$$\left(\frac{\partial}{\partial t}\right)_\sigma(m\theta)+\nabla_\sigma\cdot(m\theta\mathbf{v})+\frac{\partial}{\partial\sigma}(m\theta\dot{\sigma})=\frac{mQ}{\Pi}. \quad (2.26)$$

If we integrate (2.26) over the entire atmosphere, all terms vanish under adiabatic processes so that constraint (iii) is satisfied. Similarly, for an arbitrary function of the potential temperature $F(\theta)$, we can write

$$\left(\frac{\partial}{\partial t}\right)_\sigma[mF(\theta)]+\nabla_\sigma\cdot[mF(\theta)\mathbf{v}]$$
$$+\frac{\partial}{\partial\sigma}[mF(\theta)\dot{\sigma}]=m\frac{DF(\theta)}{Dt}. \quad (2.27)$$

As with (2.26), we see that constraint (iv) is satisfied.

3. Vertical discretization with the generalized σ coordinate based on the Charney–Phillips grid

a. Vertical grid

Arakawa (1972), Arakawa and Lamb (1977), and Arakawa and Suarez (1983) constructed vertically discrete models based on the L grid satisfying all or most of the integral constraints given in section 2b. Our objective here is to construct a vertically discrete model following a similar approach but based on the CP grid.

We divide the atmosphere into L layers identified by integer indices increasing downward (see Fig. 1b). These layers are bounded by $L+1$ interfaces identified by half-integer indices. The upper and lower boundaries of the atmosphere are placed at interfaces, which are identified by indices $1/2$ and $L+1/2$, respectively. The horizontal velocity is predicted for each layer. Following Charney and Phillips (1953), however, the temperature is predicted at the interfaces where the vertical mass flux is defined. In discretizing the equations, the simplest centered differencing will be used whenever appropriate.

b. Formulation of a vertically discrete continuity equation

We apply the continuity equation (2.6) to layer l, which is the layer bounded by interfaces $l-1/2$ and $l+1/2$. Then we may write

$$\frac{\partial m_l}{\partial t}+\nabla\cdot(m\mathbf{v})_l+\frac{1}{(\delta\sigma)_l}[(m\dot{\sigma})_{l+1/2}-(m\dot{\sigma})_{l-1/2}]=0$$
$$\text{for}\quad l=1,2,\cdots,L, \quad (3.1)$$

where, from (2.4),

$$m_l\equiv\frac{p_{l+1/2}-p_{l-1/2}}{(\delta\sigma)_l}\quad\text{for}\quad l=1,2,\cdots,L \quad (3.2)$$

and

$$(\delta\sigma)_l\equiv\sigma_{l+1/2}-\sigma_{l-1/2}\quad\text{for}\quad l=1,2,\cdots,L. \quad (3.3)$$

The boundary conditions (2.7) are now

$$(m\dot{\sigma})_{1/2}=(m\dot{\sigma})_{L+1/2}=0. \quad (3.4)$$

We predict the temperature at the interfaces by applying the thermodynamic energy equation (2.24) there. This requires another set of continuity equations applied to the interfaces. Let us assume that m for a layer represented by the interface $(l+1/2)$ is a linear combination of m for the layers above (l) and below $(l+1)$ so that we may write

$$m_{l+1/2}\equiv a_{l+1/2}m_l+b_{l+1/2}m_{l+1}, \quad (3.5)$$

where $a_{l+1/2}+b_{l+1/2}=1$ and $a_{1/2}=b_{L+1/2}=0$. Equation (3.1) then yields

$$\frac{\partial m_{l+1/2}}{\partial t}+\nabla\cdot[a_{l+1/2}(m\mathbf{v})_l+b_{l+1/2}(m\mathbf{v})_{l+1}]$$
$$+\left\{\frac{a_{l+1/2}}{(\delta\sigma)_l}[(m\dot{\sigma})_{l+1/2}-(m\dot{\sigma})_{l-1/2}]\right.$$
$$\left.+\frac{b_{l+1/2}}{(\delta\sigma)_{l+1}}[(m\dot{\sigma})_{l+3/2}-(m\dot{\sigma})_{l+1/2}]\right\}=0$$
$$\text{for}\quad l=1,2,\cdots,L-1. \quad (3.6)$$

We now express the vertical flux terms in (3.6) in the form of flux divergence by defining

$$(m\dot{\sigma})_{l+1} - (m\dot{\sigma})_l \equiv (\delta\sigma)_{l+1/2}\left\{\frac{a_{l+1/2}}{(\delta\sigma)_l}[(m\dot{\sigma})_{l+1/2} - (m\dot{\sigma})_{l-1/2}] + \frac{b_{l+1/2}}{(\delta\sigma)_{l+1}}[(m\dot{\sigma})_{l+3/2} - (m\dot{\sigma})_{l+1/2}]\right\}$$

$$\text{for} \quad l = 1, 2, \cdots, L-1. \quad (3.7)$$

When the sum $\sum_{l=1}^{L-1}$ (3.7) is taken, however, $m\dot{\sigma}$ for interior layers on the left-hand side successively cancel, leaving only $(m\dot{\sigma})_L - (m\dot{\sigma})_1$. Then, in the sum of the right-hand side, $m\dot{\sigma}$ for interior levels must also successively cancel. Thus, the sum of the coefficients on all $(m\dot{\sigma})_{l+1/2}$ in $\sum_{l=1}^{L-1}$ (3.7) must vanish so that

$$\frac{(\delta\sigma)_{l+1/2}}{(\delta\sigma)_l}a_{l+1/2} + \frac{(\delta\sigma)_{l-1/2}}{(\delta\sigma)_l}b_{l-1/2} = \frac{(\delta\sigma)_{l+3/2}}{(\delta\sigma)_{l+1}}a_{l+3/2} + \frac{(\delta\sigma)_{l+1/2}}{(\delta\sigma)_{l+1}}b_{l+1/2}$$

$$\text{for} \quad l = 2, 3, \cdots, L-2 \quad (3.8)$$

is required. This condition is satisfied by taking

$$a_{l+1/2} = \frac{1}{2}\frac{(\delta\sigma)_l}{(\delta\sigma)_{l+1/2}}, \quad b_{l+1/2} = \frac{1}{2}\frac{(\delta\sigma)_{l+1}}{(\delta\sigma)_{l+1/2}}$$

$$\text{for} \quad l = 2, 3, \cdots, L-2. \quad (3.9)$$

We also apply (3.9) to $l = 1$ and $L - 1$. Then, from (3.9) and $a_{l+1/2} + b_{l+1/2} = 1$, we can express $(\delta\sigma)_{l+1/2}$ for interior points as follows:

$$(\delta\sigma)_{l+1/2} = \frac{1}{2}[(\delta\sigma)_l + (\delta\sigma)_{l+1}]$$

$$\text{for} \quad l = 1, 2, \cdots, L-1. \quad (3.10)$$

The continuity equation (3.6) applied to interfaces can then be written as

$$\frac{\partial m_{l+1/2}}{\partial t} + \nabla\cdot(m\mathbf{v})_{l+1/2} + \frac{1}{(\delta\sigma)_{l+1/2}}[(m\dot{\sigma})_{l+1} - (m\dot{\sigma})_l] = 0$$

$$\text{for} \quad l = 1, 2, \cdots, L-1, \quad (3.11)$$

where

$$m_{l+1/2} \equiv \frac{1}{2(\delta\sigma)_{l+1/2}}[(\delta\sigma)_l m_l + (\delta\sigma)_{l+1}m_{l+1}]$$

$$\text{for} \quad l = 1, 2, \cdots, L-1, \quad (3.12)$$

$$(m\mathbf{v})_{l+1/2} \equiv \frac{1}{2(\delta\sigma)_{l+1/2}} \times [(\delta\sigma)_l(m\mathbf{v})_l + (\delta\sigma)_{l+1}(m\mathbf{v})_{l+1}]$$

$$\text{for} \quad l = 1, 2, \cdots, L-1, \quad (3.13)$$

and

$$(m\dot{\sigma})_l \equiv \frac{1}{2}[(m\dot{\sigma})_{l+1/2} + (m\dot{\sigma})_{l-1/2}]$$

$$\text{for} \quad l = 2, 3, \cdots, L-1. \quad (3.14)$$

If we choose

$$a_{L+1/2} = b_{1/2} = 1, \quad (3.15)$$

$$\frac{(\delta\sigma)_{1/2}}{(\delta\sigma)_1} = \frac{(\delta\sigma)_{L+1/2}}{(\delta\sigma)_L} = \frac{1}{2}, \quad (3.16)$$

$$m_{1/2} = m_1, \quad m_{L+1/2} = m_L, \quad (3.17)$$

$$(m\mathbf{v})_{1/2} = (m\mathbf{v})_1, \quad (m\mathbf{v})_{L+1/2} = (m\mathbf{v})_L, \quad (3.18)$$

and

$$(m\dot{\sigma})_1 = \frac{1}{2}(m\dot{\sigma})_{3/2}, \quad (m\dot{\sigma})_L = \frac{1}{2}(m\dot{\sigma})_{L-1/2}, \quad (3.19)$$

then we may write the continuity equation applied to the upper and lower boundaries

$$\frac{\partial m_{1/2}}{\partial t} + \nabla\cdot(m\mathbf{v})_1 + \frac{1}{(\delta\sigma)_1}(m\dot{\sigma})_{3/2} = 0 \quad (3.20)$$

and

$$\frac{\partial m_{L+1/2}}{\partial t} + \nabla\cdot(m\mathbf{v})_L - \frac{1}{(\delta\sigma)_L}(m\dot{\sigma})_{L-1/2} = 0, \quad (3.21)$$

respectively. We can show that, with these choices, the vertical sum of the continuity equation for layers multiplied by $(\delta\sigma)_l$ is equivalent to that for interfaces multiplied by $(\delta\sigma)_{l+1/2}$.

c. *Formulation of vertically discrete equations satisfying constraints (i) and (ii)*

The vertically discrete form of the pressure gradient force (2.22) can be written as

$$-(\nabla_p\Phi)_l = -\frac{1}{m_l}\nabla(m_l\Phi_l) + \frac{1}{m_l(\delta\sigma)_l}(\Phi_{l+1/2}\nabla p_{l+1/2} - \Phi_{l-1/2}\nabla p_{l-1/2})$$

$$\text{for} \quad l = 1, 2, \cdots, L. \quad (3.22)$$

Consider the vertically mass-weighed sum of the pressure gradient force, $\sum_{l=1}^{L}$ (3.22)$m_l(\delta\sigma)_l$. It can be written as

$$-\sum_{l=1}^{L} m_l(\nabla_p\Phi)_l(\delta\sigma)_l = -\nabla\sum_{l=1}^{L} m_l\Phi_l(\delta\sigma)_l + \Phi_S\nabla p_S. \quad (3.23)$$

Here $p_{1/2} = \text{const}$ has been used. When (3.23) is integrated along a contour of the surface of topography,

for which Φ_S is constant, the right-hand side vanishes. Therefore, constraint (i) is satisfied in the discrete system.

To satisfy constraint (ii), we first express the work done by the pressure gradient force for each layer and identify the energy conversion term $(m\alpha\omega)$ for that layer. By multiplying the discrete pressure gradient force (3.22) by $(m\mathbf{v})_l$, we obtain

$$
\begin{aligned}
-m_l\mathbf{v}_l\cdot(\nabla_p\Phi)_l &= -\nabla\cdot(m_l\mathbf{v}_l\Phi_l) + \Phi_l\nabla\cdot(m_l\mathbf{v}_l) - \Phi_l\mathbf{v}_l\cdot\nabla m_l \\
&\quad + \frac{1}{(\delta\sigma)_l}(\Phi_{l+1/2}\mathbf{v}_l\cdot\nabla p_{l+1/2} - \Phi_{l-1/2}\mathbf{v}_l\cdot\nabla p_{l-1/2}), \\
&\qquad \text{for } l = 1, 2, \cdots, L. \quad (3.24)
\end{aligned}
$$

Here we have used $(m\mathbf{v})_l \equiv m_l\mathbf{v}_l$. Substituting (3.1) and (3.2), we can rewrite (3.24) as

$$
\begin{aligned}
-m_l\mathbf{v}_l\cdot(\nabla_p\Phi)_l &= -\nabla\cdot(m_l\mathbf{v}_l\Phi_l) - \frac{1}{(\delta\sigma)_l}\left\{\Phi_{l+1/2}\left[\frac{\partial p_{l+1/2}}{\partial t} + (m\dot{\sigma})_{l+1/2}\right] - \Phi_{l-1/2}\left[\frac{\partial p_{l-1/2}}{\partial t} + (m\dot{\sigma})_{l-1/2}\right]\right\} \\
&\quad + \frac{1}{(\delta\sigma)_l}(\Phi_{l+1/2} - \Phi_l)\left[\frac{\partial p_{l+1/2}}{\partial t} + \mathbf{v}_l\cdot\nabla p_{l+1/2} + (m\dot{\sigma})_{l+1/2}\right] \\
&\quad + \frac{1}{(\delta\sigma)_l}(\Phi_l - \Phi_{l-1/2})\left[\frac{\partial p_{l-1/2}}{\partial t} + \mathbf{v}_l\cdot\nabla p_{l-1/2} + (m\dot{\sigma})_{l-1/2}\right], \quad \text{for } l = 1, 2, \cdots, L. \quad (3.25)
\end{aligned}
$$

If we compare the right-hand side of (3.25) to that of (2.25), the energy conversion term $(m\alpha\omega)_l$ can be identified as

$$
\begin{aligned}
&-\frac{1}{(\delta\sigma)_l}(\Phi_{l+1/2} - \Phi_l) \\
&\times\left[\frac{\partial p_{l+1/2}}{\partial t} + \mathbf{v}_l\cdot\nabla p_{l+1/2} + (m\dot{\sigma})_{l+1/2}\right] \\
&-\frac{1}{(\delta\sigma)_l}(\Phi_l - \Phi_{l-1/2}) \\
&\times\left[\frac{\partial p_{l-1/2}}{\partial t} + \mathbf{v}_l\cdot\nabla p_{l-1/2} + (m\dot{\sigma})_{l-1/2}\right] \\
&\qquad \text{for} \quad l = 1, 2, \cdots, L. \quad (3.26)
\end{aligned}
$$

To rewrite this term in a form that explicitly depends upon θ, we first express the discrete hydrostatic equation as

$$
\Phi_l - \Phi_{l+1/2} \equiv A_{l+1/2}\theta_{l+1/2} \quad \text{for} \quad l = 1, 2, \cdots, L \quad (3.27)
$$

and

$$
\begin{aligned}
&\Phi_{l+1/2} - \Phi_{l+1} \equiv B_{l+1/2}\theta_{l+1/2} \\
&\qquad \text{for} \quad l = 0, 1, 2, \cdots, L-1, \quad (3.28)
\end{aligned}
$$

where $A_{l+1/2}$ and $B_{l+1/2}$ remain to be specified. Then the thickness between the two adjacent layers is given by

$$
\begin{aligned}
&\Phi_l - \Phi_{l+1} = (A_{l+1/2} + B_{l+1/2})\theta_{l+1/2} \\
&\qquad \text{for} \quad l = 1, 2, \cdots, L-1, \quad (3.29)
\end{aligned}
$$

which depends on θ at the interface of the two adjacent layers. In this aspect, (3.29) differs from the usual discrete hydrostatic equation based on the L grid, in which the thickness between two adjacent layers depends on an average of θ for the two layers. As we discussed in section 1, this averaging allows the existence of a computational mode. Using (3.27) and (3.28) in (3.25), we can define the energy conversion term $(m\alpha\omega)_l$ as

$$
\begin{aligned}
(m\alpha\omega)_l &\equiv \frac{1}{(\delta\sigma)_l}A_{l+1/2}\theta_{l+1/2} \\
&\quad\times\left[\frac{\partial p_{l+1/2}}{\partial t} + \mathbf{v}_l\cdot\nabla p_{l+1/2} + (m\dot{\sigma})_{l+1/2}\right] + \frac{1}{(\delta\sigma)_l} \\
&\quad\times B_{l-1/2}\theta_{l-1/2}\left[\frac{\partial p_{l-1/2}}{\partial t} + \mathbf{v}_l\cdot\nabla p_{l-1/2} + (m\dot{\sigma})_{l-1/2}\right] \\
&\qquad \text{for} \quad l = 1, 2, \cdots, L. \quad (3.30)
\end{aligned}
$$

Now we discretize the thermodynamic energy equation (2.24) applied to the interfaces in such a way that constraint (ii) is satisfied. We first write

$$
\begin{aligned}
&\frac{\partial}{\partial t}(m_{l+1/2}c_pT_{l+1/2}) + \nabla\cdot[(m\mathbf{v})_{l+1/2}c_pT_{l+1/2}] \\
&\quad + \frac{c_p}{(\delta\sigma)_{l+1/2}}[(Tm\dot{\sigma})_{l+1} - (Tm\dot{\sigma})_l] \\
&\quad = (m\alpha\omega)_{l+1/2} + (mQ)_{l+1/2} \\
&\qquad \text{for} \quad l = 1, 2, \cdots, L-1. \quad (3.31)
\end{aligned}
$$

For the upper and lower boundaries, we write

$$
\begin{aligned}
&\frac{\partial}{\partial t}(m_{1/2}c_pT_{1/2}) + \nabla\cdot[(m\mathbf{v})_1c_pT_{1/2}] \\
&\quad + \frac{c_p}{(\delta\sigma)_{1/2}}(Tm\dot{\sigma})_1 = (m\alpha\omega)_{1/2} + (mQ)_{1/2} \quad (3.32)
\end{aligned}
$$

and

$$\frac{\partial}{\partial t} m_{L+1/2} c_p T_{L+1/2} + \nabla\cdot[(m\mathbf{v})_L c_p T_{L+1/2}] - \frac{c_p}{(\delta\sigma)_{L+1/2}} (Tm\dot{\sigma})_L = (m\alpha\omega)_{L+1/2} + (mQ)_{L+1/2}. \quad (3.33)$$

Here $(m\mathbf{v})_{l+1/2}$ is defined by (3.13) and (3.18). The expression for $(Tm\dot{\sigma})_l$ remains to be specified. Constraint (ii) requires that the vertical sum of the energy conversion term $(m\alpha\omega)(\delta\sigma)$ in the kinetic energy equation and that in the thermodynamic energy equation be equal. Then

$$\sum_{l=1}^{L} (m\alpha\omega)_l(\delta\sigma)_l = \sum_{l=0}^{L} (m\alpha\omega)_{l+1/2}(\delta\sigma)_{l+1/2}. \quad (3.34)$$

The term $(m\alpha\omega)_l(\delta\sigma)_l$ on the left-hand side is given by (3.30). From this expression, we can identify the contribution of $\theta_{l+1/2}$ to the energy conversion in the layer (l). Similarly, from (3.30) with l increased by one, we can identify the contribution of $\theta_{l+1/2}$ to the energy conversion in the layer $(l+1)$. Then, to satisfy (3.34), we express

$$(m\alpha\omega)_{l+1/2}(\delta\sigma)_{l+1/2} = \theta_{l+1/2}\left\{(A_{l+1/2} + B_{l+1/2})\left[\frac{\partial p_{l+1/2}}{\partial t} + (m\dot{\sigma})_{l+1/2}\right] + (A_{l+1/2}\mathbf{v}_l + B_{l+1/2}\mathbf{v}_{l+1})\cdot\nabla p_{l+1/2}\right\} \quad \text{for} \quad l = 1, 2, \cdots, L-1, \quad (3.35)$$

$$(m\alpha\omega)_{1/2}(\delta\sigma)_{1/2} = \theta_{1/2}B_{1/2} \times \left[\left(\frac{\partial p_{1/2}}{\partial t}\right) + \mathbf{v}_1\cdot\nabla p_{1/2}\right] = 0, \quad (3.36)$$

and

$$(m\alpha\omega)_{L+1/2}(\delta\sigma)_{L+1/2} = \theta_{L+1/2}A_{L+1/2}\left[\left(\frac{\partial p_{L+1/2}}{\partial t}\right) + \mathbf{v}_L\cdot\nabla p_{L+1/2}\right]. \quad (3.37)$$

In (3.36) and (3.37), we have used (3.4). With (3.35)–(3.37), the thermodynamic energy equations given by (3.31)–(3.33) satisfy constraint (ii) regardless of the choices for $A_{l+1/2}$, $B_{l+1/2}$ and $(Tm\dot{\sigma})_l$.

d. Further specification of the vertically discrete thermodynamic equation

To specify the unspecified variables in the discrete thermodynamic equations derived above, we first rewrite (3.31)–(3.33) using

$$c_p T_{l+1/2} = \Pi_{l+1/2}\theta_{l+1/2} \quad \text{with} \quad \Pi_{l+1/2} \equiv c_p(p_{l+1/2}/p_0)^\kappa \quad \text{for} \quad l = 0, 1, 2, \cdots, L \quad (3.38)$$

and the continuity equations (3.11), (3.20), and (3.21). After rearranging terms, we obtain

$$\Pi_{l+1/2}\left[m_{l+1/2}\frac{\partial\theta_{l+1/2}}{\partial t} + (m\mathbf{v})_{l+1/2}\cdot\nabla\theta_{l+1/2}\right] + \theta_{l+1/2}\left(\frac{\partial\Pi_{l+1/2}}{\partial p_{l+1/2}}\right)\left[m_{l+1/2}\frac{\partial p_{l+1/2}}{\partial t} + (m\mathbf{v})_{l+1/2}\cdot\nabla p_{l+1/2}\right]$$
$$= \frac{c_p T_{l+1/2}}{(\delta\sigma)_{l+1/2}}[(m\dot{\sigma})_{l+1} - (m\dot{\sigma})_l] - \frac{c_p}{(\delta\sigma)_{l+1/2}}[(Tm\dot{\sigma})_{l+1} - (Tm\dot{\sigma})_l]$$
$$+ \frac{\theta_{l+1/2}}{(\delta\sigma)_{l+1/2}}\left\{(A_{l+1/2} + B_{l+1/2})\left[\frac{\partial p_{l+1/2}}{\partial t} + (m\dot{\sigma})_{l+1/2}\right] + (A_{l+1/2}\mathbf{v}_l + B_{l+1/2}\mathbf{v}_{l+1})\cdot\nabla p_{l+1/2}\right\} + (mQ)_{l+1/2}$$
$$\text{for} \quad l = 1, 2, \cdots, L-1; \quad (3.39)$$

$$\Pi_{1/2}\left[m_{1/2}\frac{\partial\theta_{1/2}}{\partial t} + (m\mathbf{v})_{1/2}\cdot\nabla\theta_{1/2}\right] + \theta_{1/2}\left(\frac{\partial\Pi_{1/2}}{\partial p_{1/2}}\right)\left[m_{1/2}\frac{\partial p_{1/2}}{\partial t} + (m\mathbf{v})_{1/2}\cdot\nabla p_{1/2}\right] = \frac{c_p T_{1/2}}{(\delta\sigma)_{1/2}}(m\dot{\sigma})_1 - \frac{c_p}{(\delta\sigma)_{1/2}}(Tm\dot{\sigma})_1 + (mQ)_{1/2}; \quad (3.40)$$

and

$$\Pi_{L+1/2}\left[m_{L+1/2}\frac{\partial\theta_{L+1/2}}{\partial t} + (m\mathbf{v})_{L+1/2}\cdot\nabla\theta_{L+1/2}\right] + \theta_{L+1/2}\left(\frac{\partial\Pi_{L+1/2}}{\partial p_{L+1/2}}\right)\left[m_{L+1/2}\frac{\partial p_{L+1/2}}{\partial t} + (m\mathbf{v})_{L+1/2}\cdot\nabla p_{L+1/2}\right]$$
$$= -\frac{c_p T_{L+1/2}}{(\delta\sigma)_{L+1/2}}(m\dot{\sigma})_L + \frac{c_p}{(\delta\sigma)_{L+1/2}}(Tm\dot{\sigma})_L + \theta_{L+1/2}A_{L+1/2}\left[\left(\frac{\partial p_{L+1/2}}{\partial t}\right) + \mathbf{v}_L\cdot\nabla p_{L+1/2}\right] + (mQ)_{L+1/2}. \quad (3.41)$$

By comparing (3.39)–(3.41) to (2.12), we first require that the terms involving $\partial p_{l+1/2}/\partial t$ and $\nabla p_{l+1/2}$ vanish. This can be achieved by choosing $A_{l+1/2}$ and $B_{l+1/2}$ as

$$A_{l+1/2} \equiv \frac{(\delta\sigma)_l m_l}{2}\left(\frac{\partial \Pi_{l+1/2}}{\partial p_{l+1/2}}\right) \quad \text{for} \quad l = 1, 2, \cdots, L, \quad (3.42)$$

$$B_{l+1/2} \equiv \frac{(\delta\sigma)_{l+1} m_{l+1}}{2}\left(\frac{\partial \Pi_{l+1/2}}{\partial p_{l+1/2}}\right) \quad \text{for} \quad l = 0, 1, 2, \cdots, L-1 \quad (3.43)$$

and using (3.12), (3.13), (3.17) and (3.18). Substitution of (3.42) and (3.43) in (3.39)–(3.41) gives

$$\Pi_{l+1/2}\left[m_{l+1/2}\frac{\partial \theta_{l+1/2}}{\partial t} + (m\mathbf{v})_{l+1/2}\cdot\nabla\theta_{l+1/2}\right] = \frac{c_p T_{l+1/2}}{(\delta\sigma)_{l+1/2}}[(m\dot\sigma)_{l+1} - (m\dot\sigma)_l] - \frac{c_p}{(\delta\sigma)_{l+1/2}}[(Tm\dot\sigma)_{l+1} - (Tm\dot\sigma)_l]$$
$$+ \frac{\theta_{l+1/2}}{(\delta\sigma)_{l+1/2}} m_{l+1/2}\left(\frac{\partial \Pi_{l+1/2}}{\partial p_{l+1/2}}\right)(m\dot\sigma)_{l+1/2} + (mQ)_{l+1/2} \quad \text{for} \quad l = 1, 2, \cdots, L-1; \quad (3.44)$$

$$\Pi_{1/2}\left[m_{1/2}\frac{\partial \theta_{1/2}}{\partial t} + (m\mathbf{v})_{1/2}\cdot\nabla\theta_{1/2}\right] = \frac{c_p T_{1/2}}{(\delta\sigma)_{1/2}}(m\dot\sigma)_1 - \frac{c_p}{(\delta\sigma)_{1/2}}(Tm\dot\sigma)_1 + (mQ)_{1/2}; \quad (3.45)$$

and

$$\Pi_{L+1/2}\left[m_{L+1/2}\frac{\partial \theta_{L+1/2}}{\partial t} + (m\mathbf{v})_{L+1/2}\cdot\nabla\theta_{L+1/2}\right] = -\frac{c_p T_{L+1/2}}{(\delta\sigma)_{L+1/2}}(m\dot\sigma)_L + \frac{c_p}{(\delta\sigma)_{L+1/2}}(Tm\dot\sigma)_L + (mQ)_{L+1/2}. \quad (3.46)$$

Next, we identify the term representing the vertical advection of the potential temperature, $[(m\dot\sigma)(\partial\theta/\partial\sigma)]_{l+1/2}$. Unlike the L grid, the use of the CP grid allows us to express the vertical advection of the potential temperature in terms of the vertical mass flux at that level alone. Maintaining this advantage is important since, with this choice, conservation of the quasigeostrophic potential vorticity for quasigeostrophic flow and that of the potential temperature at the vertical boundaries under adiabatic processes can be maintained as in the vertically discrete quasigeostrophic system of equations by Charney and Phillips (1953). Therefore, we express the discrete thermodynamic equation as

$$\left[m_{l+1/2}\frac{\partial \theta_{l+1/2}}{\partial t} + (m\mathbf{v})_{l+1/2}\cdot\nabla\theta_{l+1/2}\right] + (m\dot\sigma)_{l+1/2}\left(\frac{\partial\theta}{\partial\sigma}\right)_{l+1/2} = \frac{(mQ)_{l+1/2}}{\Pi_{l+1/2}} \quad \text{for} \quad l = 1, 2, \cdots, L-1, \quad (3.47)$$

$$m_{1/2}\frac{\partial \theta_{1/2}}{\partial t} + (m\mathbf{v})_1\cdot\nabla\theta_{1/2} = \frac{(mQ)_{1/2}}{\Pi_{1/2}}, \quad (3.48)$$

and

$$m_{L+1/2}\frac{\partial \theta_{L+1/2}}{\partial t} + (m\mathbf{v})_L\cdot\nabla\theta_{L+1/2} = \frac{(mQ)_{L+1/2}}{\Pi_{L+1/2}}. \quad (3.49)$$

To obtain a specific form for $(\partial\theta/\partial\sigma)_{l+1/2}$, we substitute (3.47)–(3.49) into (3.44)–(3.46) to eliminate the terms involving $\partial\theta_{l+1/2}/\partial t$ and $(m\mathbf{v})_{l+1/2}\cdot\nabla\theta_{l+1/2}$. The resulting equations after these eliminations together with (3.14) and (3.19) give a requirement on the relation between the unspecified $(m\dot\sigma)_{l+1/2}(\partial\theta/\partial\sigma)_{l+1/2}$, $(Tm\dot\sigma)_{l+1} - (Tm\dot\sigma)_l$ and $T_{l+1/2}[(m\dot\sigma)_{l+3/2} - (m\dot\sigma)_{l-1/2}]$. We find that the following choice satisfies the requirement

$$(Tm\dot\sigma)_l \equiv \frac{1}{2}[T_{l-1/2}(m\dot\sigma)_{l+1/2} + T_{l+1/2}(m\dot\sigma)_{l-1/2}] \quad \text{for} \quad l = 1, 2, \cdots, L-1. \quad (3.50)$$

Then we can define

$$\left[(m\dot\sigma)\left(\frac{\partial\theta}{\partial\sigma}\right)\right]_{l+1/2} \equiv \frac{(m\dot\sigma)_{l+1/2}}{\Pi_{l+1/2}(\delta\sigma)_{l+1/2}}\left[c_p\frac{T_{l+3/2} - T_{l-1/2}}{2} - (\delta\sigma)_{l+1/2} m_{l+1/2}\left(\frac{\partial \Pi_{l+1/2}}{\partial p_{l+1/2}}\right)\theta_{l+1/2}\right] \quad \text{for} \quad l = 1, 2, \cdots, L-1. \quad (3.51)$$

The coefficient on $(m\dot\sigma)_{l+1/2}$ in the right-hand side of this equation is a finite-difference analog of $\partial\theta/\partial\sigma \equiv (c_p\partial T/\partial\sigma - m\theta\partial\Pi/\partial p)\Pi^{-1}$.

e. Vertically discrete pressure tendency and mass-flux equations

Substituting (3.2) in (3.1) and summing the result multiplied by $(\delta\sigma)_l$ from the top of the atmosphere ($l = 1$) to the layer l, we can write the pressure tendency equation as

$$\frac{\partial p_{l+1/2}}{\partial t} = -\sum_{k=1}^{l} \nabla\cdot(m\mathbf{v})_k(\delta\sigma)_k - (m\dot{\sigma})_{l+1/2}$$

$$\text{for} \quad l = 1, 2, \cdots, L-1, \quad (3.52)$$

where we have used (3.4). Applying (3.52) to $l = L$ and using (3.4), we can write the surface pressure tendency equation as

$$\frac{\partial p_S}{\partial t} = -\sum_{k=1}^{L} \nabla\cdot(m\mathbf{v})_k(\delta\sigma)_k, \quad (3.53)$$

where $p_S \equiv p_{L+1/2}$.

Differentiating

$$\sigma_{l+1/2} \equiv F(p_{l+1/2}, p_S) \quad \text{for} \quad l = 0, 1, 2, \cdots, L, \quad (3.54)$$

with respect to t and requiring $\partial\sigma_{l+1/2}/\partial t = 0$, we can write

$$\left(\frac{\partial F}{\partial p}\right)_{l+1/2} \frac{\partial p_{l+1/2}}{\partial t} + \left(\frac{\partial F}{\partial p_S}\right)_{l+1/2} \frac{\partial p_S}{\partial t} = 0$$

$$\text{for} \quad l = 0, 1, 2, \cdots, L. \quad (3.55)$$

Using (3.52) and (3.53) in (3.55), the diagnostic equation to determine the vertical mass flux can be obtained as

$$-\left(\frac{\partial F}{\partial p}\right)_{l+1/2} (m\dot{\sigma})_{l+1/2} = \left(\frac{\partial F}{\partial p}\right)_{l+1/2} \sum_{k=1}^{l} \nabla\cdot(m\mathbf{v})_k(\delta\sigma)_k + \left(\frac{\partial F}{\partial p_S}\right)_{l+1/2} \sum_{k=1}^{L} \nabla\cdot(m\mathbf{v})_k(\delta\sigma)_k$$

$$\text{for} \quad l = 1, 2, \cdots, L-1. \quad (3.56)$$

On the other hand, the vertical mass flux at the upper and lower boundaries is given by (3.4).

f. Choices for $\sigma = F(p, p_S)$

The model presented in section 2 is based on a generalized σ coordinate, $\sigma = F(p, p_S)$, that can be used as the p coordinate, the standard σ coordinate, or any hybrid combination of these two, provided that σ changes monotonically with height and is constant at the top and bottom boundaries. The primary purpose for using a generalized σ coordinate is to use the advantages of the σ coordinate in handling the surface topography while minimizing the errors due to the steep topography away from the surface. A broad family of such coordinates can be obtained by taking a linear combination of $(p - p_T)(p_S - p_T)^{-1}$ and $f(p)$, given by

$$\sigma \equiv F(p, p_S) = a(p, p_S)\left(\frac{p - p_T}{p_S - p_T}\right) + [1 - a(p, p_S)]f(p), \quad (3.57)$$

as long as σ monotonically changes in height. Here $a(p, p_S)$ is a function satisfying $1 \geq a(p, p_S) \geq 0$ for $p_S \geq p \geq p_T$. If we choose $a = 1$ and $p_T = 0$, the coordinate is identical to the original σ coordinate proposed by Phillips (1957). On the other hand, if we choose $a(p, p_S) \equiv p/p_S$, $p_T = 0$ and $f(p) \equiv p/p_C$, where p_C is a constant, the coordinate is identical to the hybrid vertical coordinate used by Simmons and Burridge (1981).

A summary of the system of discrete equations based on the generalized σ coordinate is given in appendix A.

4. Numerical simulations with the L grid and the CP grid

a. Simulation of standing waves

To demonstrate the existence of the computational mode in the L grid, we use the linearized versions of two models with the simplest centered vertical differencing on the p coordinate, one based on the L grid and the other on the CP grid. To simulate horizontally standing waves superimposed on a resting isothermal ($T_0 = 250$ K) basic state on an f plane, we perform two sets of integrations, the first from unbalanced initial perturbations and the second from no initial perturbations but forced by diabatic heating. A detailed description of the model equations are given in appendix B. We use 40 layers equally spaced in $\ln p$ below 1 mb.

In the first set of simulations, the initial conditions consist of wave perturbations in θ' with 0.5-K amplitude and opposite sign at two adjacent levels (39 and 38 for the L grid case and for 39.5 and 38.5 for the CP-grid case) and $\theta' = 0$ everywhere else. Figure 3 shows the time evolution of the amplitudes of θ' in the lower part of the domain for two horizontal wavelengths, $L = 100$ and 250 km. In the L-grid simulation, the flow is dominated by stationary components for the two wavelengths. The vertically propagating oscillatory component is weak in this case, having significant amplitudes only during early hours of the simulations. The CP-grid simulations, on the other hand, clearly show vertical propagations and almost complete dispersion of initial perturbations after 24 h.

In the second set of simulations, the initial conditions consist of $\theta' = 0$ everywhere. A Newtonian-type diabatic heating term based on a time-independent equilibrium value of θ (θ^*) with an amplitude of 10 K is added to the equations with a coefficient of 1 day^{-1} for level 37 in the L-grid case and for level 37.5 in the CP-grid case. Figure 4 shows the time evolution of the amplitudes of θ' in the lower part of the domain for two horizontal wavelengths. In the L-grid simulations,

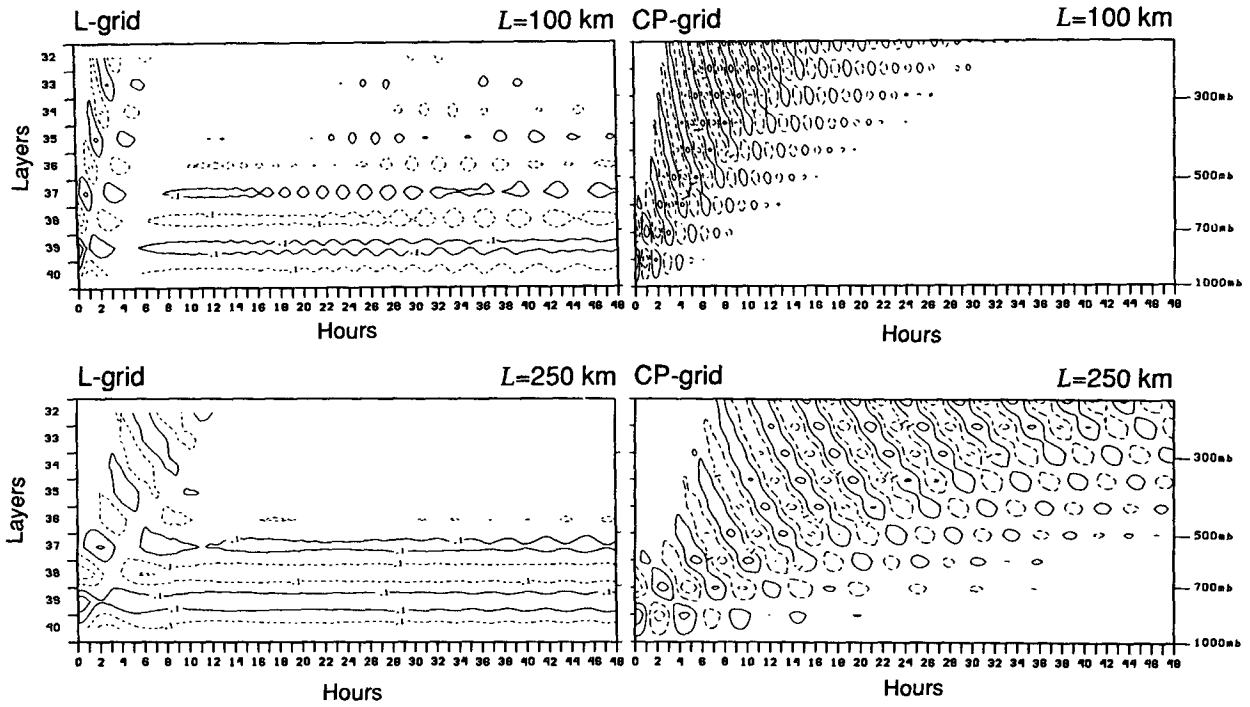

FIG. 3. Time evolution of the potential temperature perturbation θ' (K) in the lower portion of the vertical domain obtained from the models based on the Lorenz (left panels) and Charney–Phillips (right panels) grids for horizontal wavelengths L = 100 km (upper panels) and L = 250 km (lower panels). Simulations are started from unbalanced θ' at two adjacent levels with opposite signs. Solid and dashed lines correspond to positive and negative values, respectively. The contour interval is 0.2 K starting from ±0.1 K.

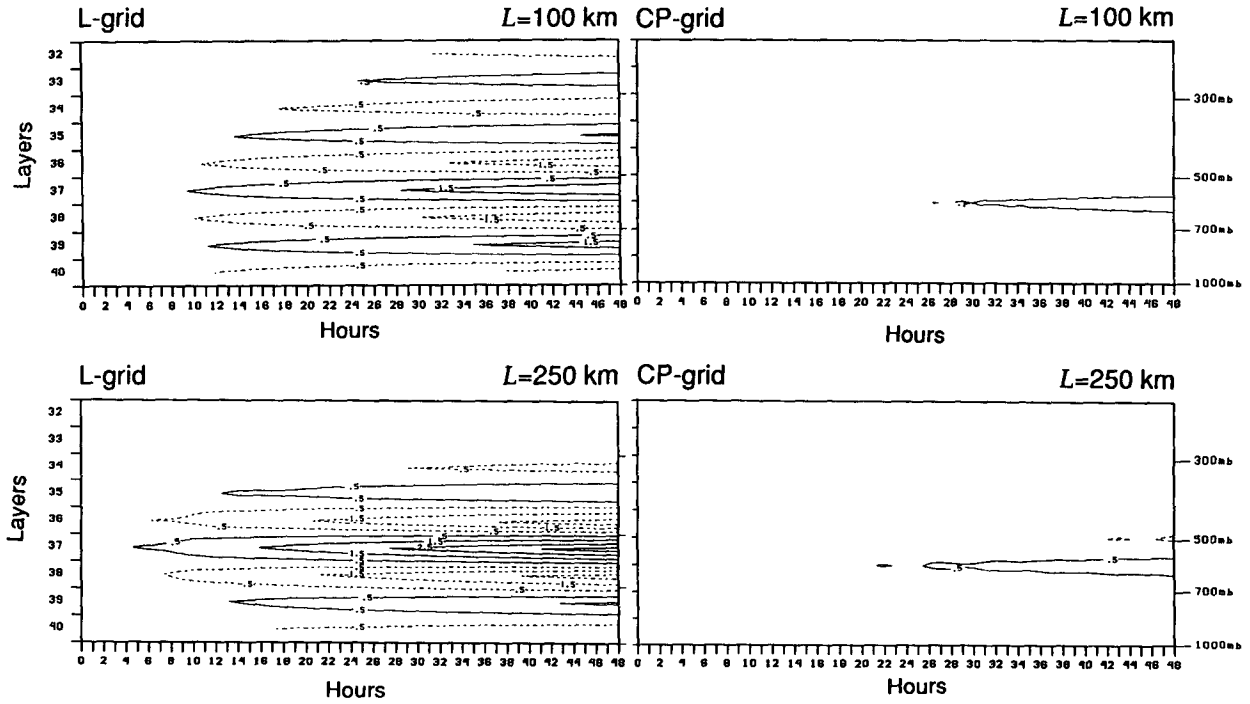

FIG. 4. As in Fig. 3 but simulations are forced by a Newtonian-type heating at a single level. The contour interval is 1.0 K starting from ±0.5 K, except the solid line represents +0.1 K in the upper-right panel.

we see the generation of vertically zigzag distribution of θ. We also see that the warming (or cooling) at the levels with heating is not sufficiently compensated by the adiabatic cooling (or warming) of the ascending (or descending) motion. In the CP-grid simulations, however, the rates of warming and cooling are much smaller due to the compensation.

b. *Simulation of baroclinic disturbance*

Arakawa and Moorthi (1988) discussed the spurious baroclinic instability for short waves with the L grid. They demonstrated the growth of short waves using a primitive equation model based on the L grid in a σ coordinate. Here we present a comparison of similar simulations obtained by two σ-coordinate models, one based on the L grid and the other on the CP grid. The vertical differencing in the L-grid model follows Arakawa and Suarez (1983) and that in the CP-grid model follows the discrete equations derived in section 3 and summarized in appendix A. The horizontal finite-differencing follows Arakawa and Hsu (1990) and Hsu and Arakawa (1990) in both models. The model domain is a 5000-km-long by 9000-km-wide channel on a β plane centered at 45°N. In these simulations, the horizontal grid distance is 100 km, and there are 20 layers in the vertical below $p_T = 0.1$ mb equally spaced in $\sigma \equiv (p - p_T)(p_S - p_T)^{-1}$. No physical processes except dry convective adjustment is included. Initial conditions consist of a baroclinic zonal jet in a geostrophic balance (Fig. 5) and *random perturbations* on the θ field with the magnitude in the range of ± 1 K applied to all grid points at all levels.

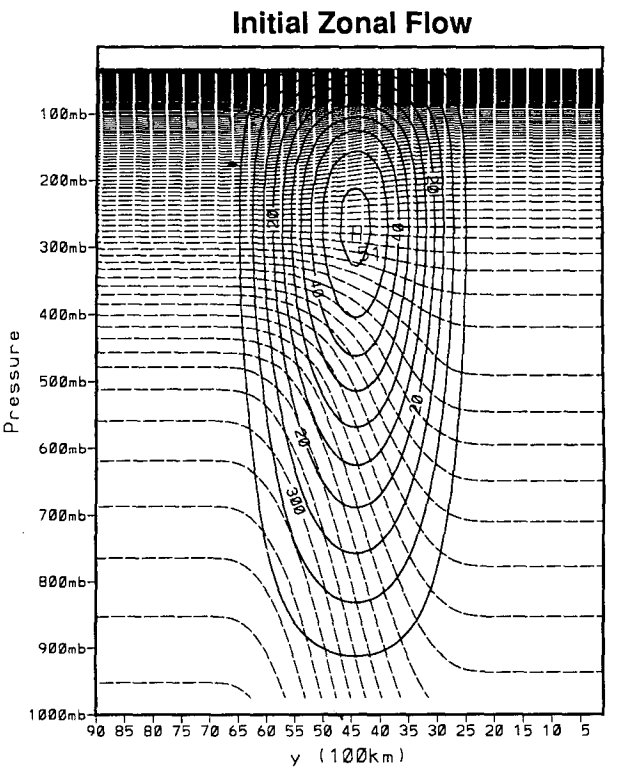

FIG. 5. Zonal component of the initial flow for the Lorenz and Charney–Phillips grid simulations. The zonal velocity (m s^{-1}) and the potential temperature (K) shown with solid and dashed lines, respectively. Contour intervals are 5 m s^{-1} for the zonal velocity and 10 K for the potential temperature, respectively.

Figure 6 shows the geopotential height and potential temperature fields obtained by the two models interpolated to the 900 mb for day 11 of the simulations. We clearly see that the simulation obtained with the L grid is dominated by short waves, particularly in the potential temperature field. A side effect of the rapid growth of short waves with the L grid is the generation of large-amplitude gravity waves. In the CP-grid simulation, there is no symptom of the spurious baroclinic instability of short waves.

Figure 7 shows the geopotential height and potential temperature fields interpolated to 900 mb for day 11 obtained by the two models with a second-order diffusion term included in the thermodynamic equation using three different coefficients $K = 10^4$, 10^5, and 10^6 m^2 s^{-1}. In the L-grid simulation, the low value of the coefficient (10^4 m^2 s^{-1}) appears to be insufficient to damp short waves (Fig. 7a), while the highest value of the coefficient (10^6 m^2 s^{-1}) causes the excessive damping of even the large-scale waves (Fig. 7c). The intermediate value of the coefficient ($K = 10^5$ m^2 s^{-1}) appears sufficient to diffuse short waves (Fig. 7b). As the short waves are damped, however, a cutoff low appears (Fig. 7b), while the simulation without diffusion does not have two separate lows (Fig. 6a). A relatively weak cutoff low also appears even with the low value of the coefficient ($K = 10^4$ m^2 s^{-1}, see Fig. 7a). In the CP-grid simulations, on the other hand, there is no significant differences in the large-scale flow with and without diffusion (see Figs. 6b, 7d and 7e) except with the large coefficient. In these cases, the diffusion acts to smooth small scales, which are mostly introduced by the initial random perturbations.

Figure 8 shows the geopotential height and potential temperature fields for day 11, interpolated to 900 mb, simulated with a fourth-order diffusion term using three coefficients 10^{14}, 10^{15}, and 10^{16} m^4 s^{-1}. In the L-grid simulations, the fourth-order diffusion effectively damps small scales as expected (Figs. 8a–c). However, changes in the large-scale flow still exist in more or less the same way as we see in the second-order diffusion simulations. In the CP grid simulations, on the other hand, the changes due to the inclusion of the fourth-order diffusion are very small in the large-scale flow (Figs. 8d–f). These simulations verify that, while the diffusion smoothes small-scale waves as expected, it also influences the large-scale flow structure with the L grid. The effect of diffusion in the CP grid simulations, on the other hand, is almost entirely limited to

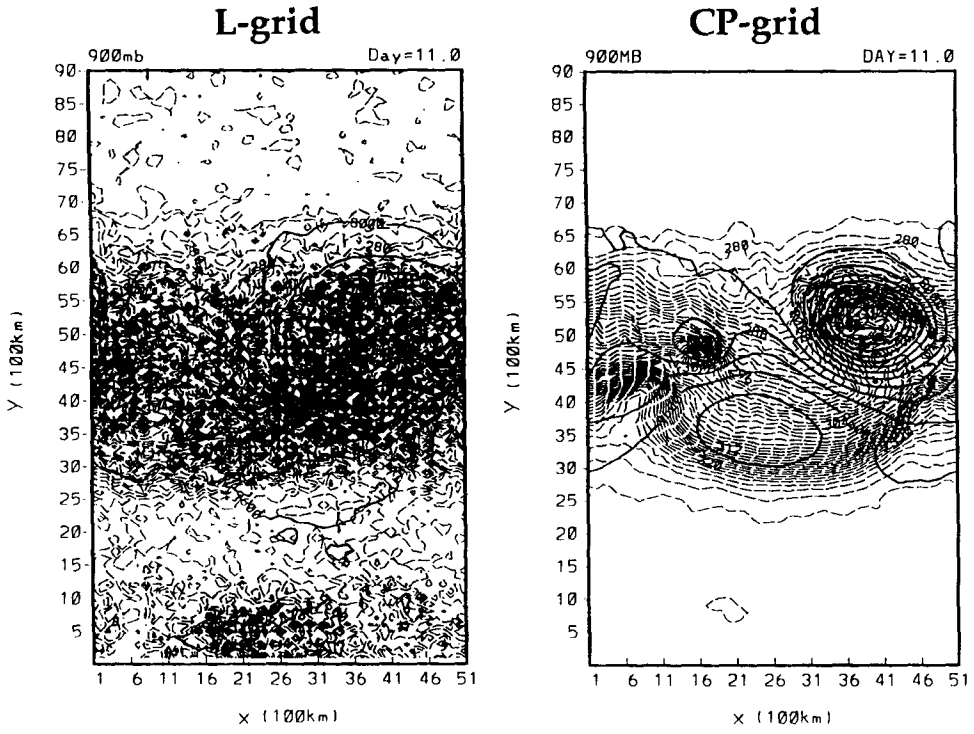

FIG. 6. The geopotential height (gpm; solid lines) and the potential temperature (K; dashed lines) interpolated to 900 mb for day 11 obtained from the models based on the Lorenz grid (left) and the Charney–Phillips grid (right). Contour intervals are 400 gpm for the geopotential height and 1 K for the potential temperature, respectively.

small scales, unless the diffusion coefficient is very large.

5. Conclusions and summary

With the L grid, the atmospheric models based on the primitive equations have two major disadvantages. One is the existence of a computational mode in the vertical thermal structure, and the other is the rapid amplification of short waves due to spurious baroclinic instability. The existence of the computational mode is a characteristic of the L grid itself, rather than that of a particular finite-difference scheme used. It exists because any straightforward finite-difference scheme for the hydrostatic equation to determine the thickness between two adjacent layers must use an average of the potential temperatures of these layers. The averaging does not allow the zigzag vertical structure of the potential temperature to affect the thickness, and, therefore, they are decoupled from the dynamics.

The rapidly amplifying short waves with the L grid are not computational modes in the above sense. They are physical modes and grow through spurious satisfaction of the necessary condition for baroclinic instability near the vertical boundaries (Arakawa and Moorthi 1988).

In this paper we construct vertical finite-difference schemes for the primitive equations based on the CP grid that maintain most of the advantages of the L grid while eliminating its disadvantages. To maintain the advantages of the CP grid, we require that in the discrete hydrostatic equation the thickness between two adjacent model layers solely depends upon the potential temperature at the interface of these layers. With this requirement, there is no room for the computational mode. We also require that the discrete vertical advection of the potential temperature be expressed solely in terms of the vertical mass flux at that level. With this requirement, the scheme reduces to that of Charney and Phillips (1953) for quasigeostrophic flow, which conserves the quasigeostrophic potential vorticity.

The finite-difference scheme presented here satisfies constraints (i) and (ii) of Arakawa and Lamb (1977), along with maintaining the advantages of the CP grid. With this scheme, the vertical advection of the potential temperature does not exactly vanish for an isentropic atmosphere. We believe that this is a minor disadvantage, however, compared to the advantages gained.

We present the results of two sets of numerical simulations using two linearized primitive equation models with the p coordinate, one using the L grid and the other using the CP grid, to simulate horizontally standing waves. In the first set, an unbalanced initial state gen-

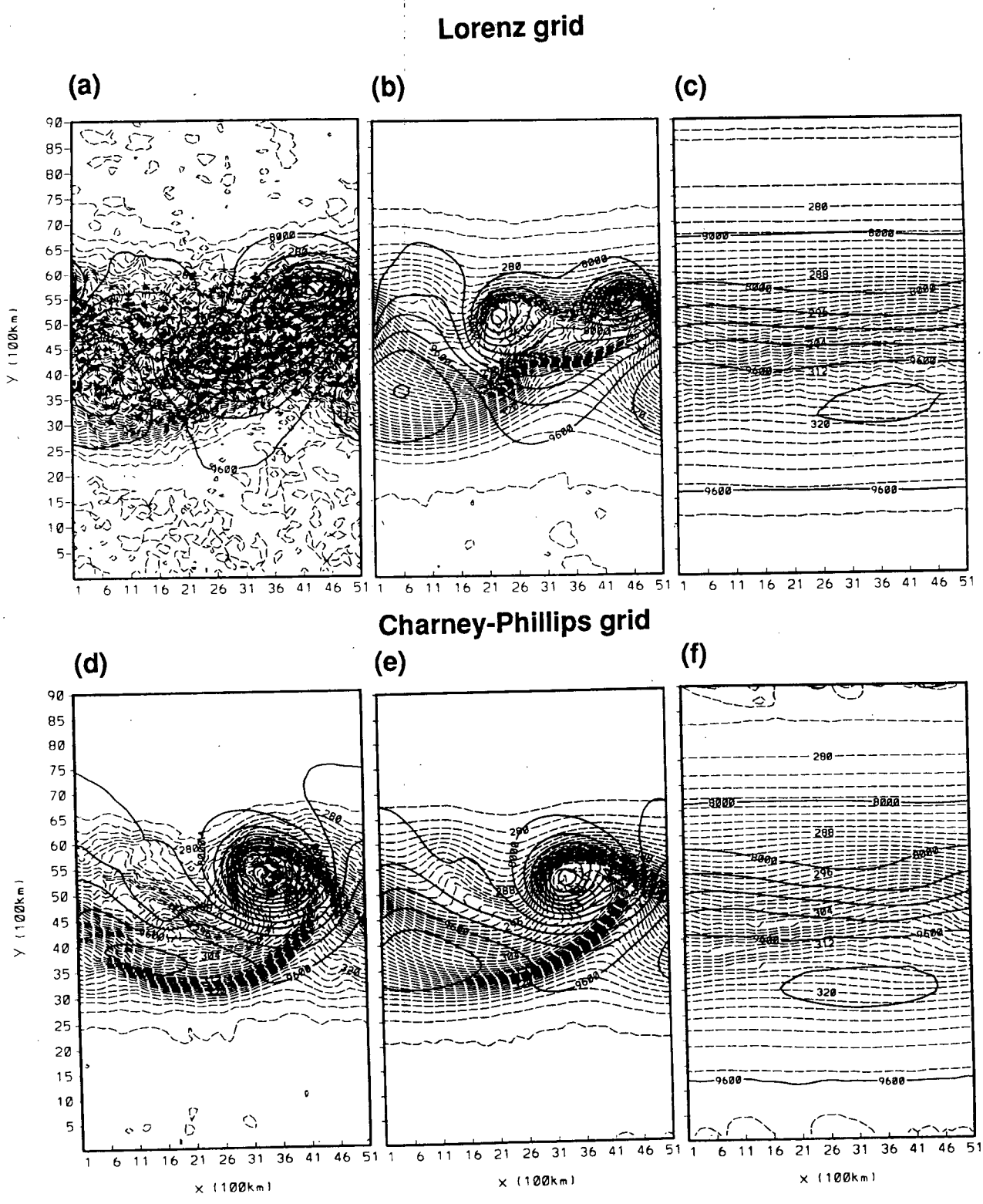

FIG. 7. As in Fig. 6 but the models include a second-order diffusion with coefficients (a), (d) 10^4 m^2 s^{-1}, (b), (e) 10^5 m^2 s^{-1}, and (c), (f) 10^6 m^2 s^{-1}. Upper panels (a), (b), (c) and lower panels (d), (e), (f) are for the Lorenz and Charney–Phillips grids, respectively.

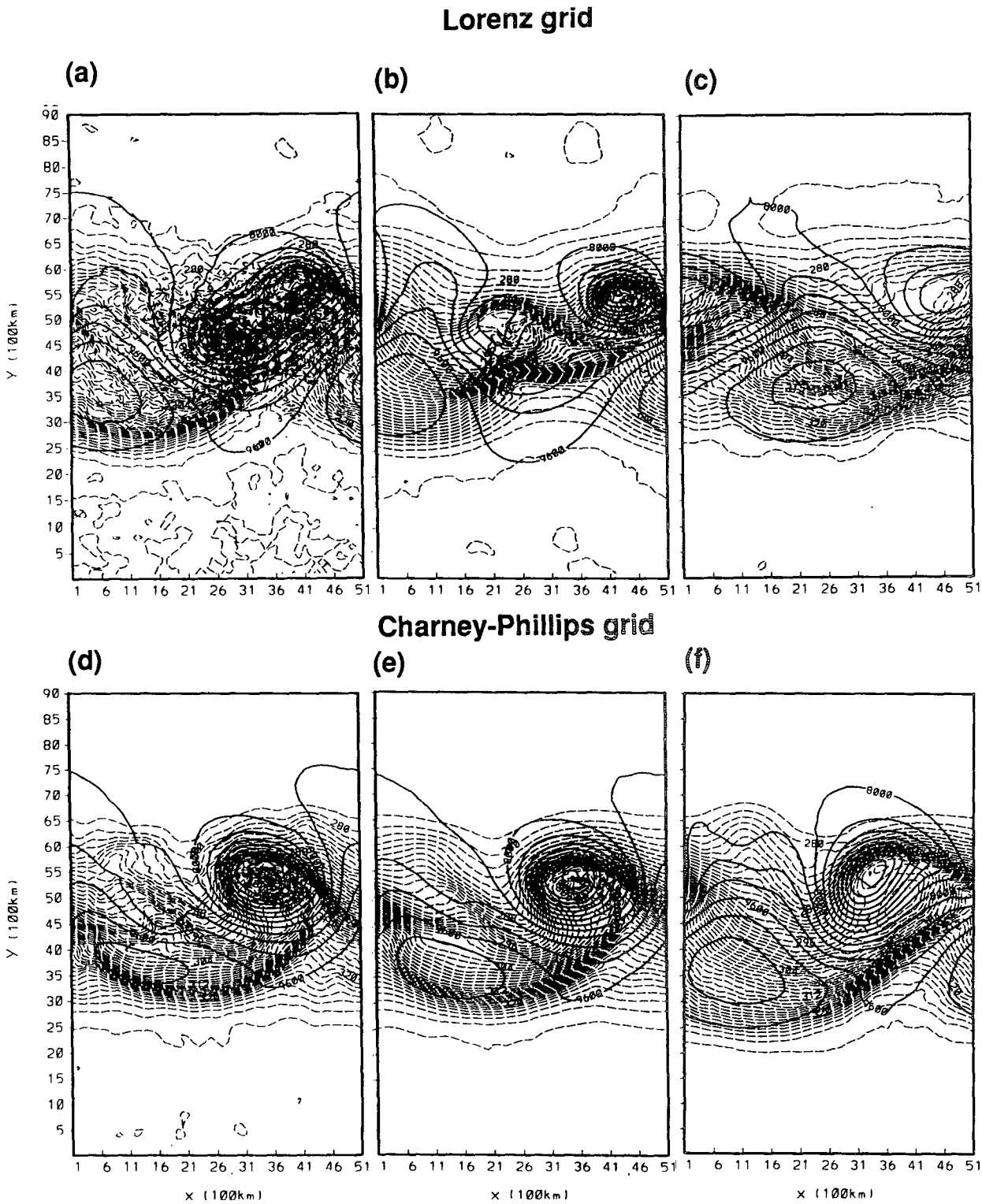

FIG. 8. As in Fig. 7 but with a fourth-order diffusion with coefficients (a), (d) 10^{14} m^4 s^{-1}, (b), (e) 10^{15} m^4 s^{-1}, and (c), (f) 10^{16} m^4 s^{-1}.

erates waves. In the second set, diabatic heating forces waves. Simulations with the L grid in the first set show the existence of the stationary computational mode, while the CP grid simulations are dominated by the vertically propagating modes.

To demonstrate the spurious baroclinic instability of short waves with the L grid, we use two σ-coordinate models, one using the L grid and the other one using the CP grid. These models differ only in the vertical discretization; otherwise they are identical. Simulations start from the same initial condition, which consist of a balanced baroclinic jet and *random perturbations* on the potential temperature field. The L-grid simulation shows rapid amplification of short waves, which dominate in the potential temperature field, while there is no similar symptom of the growth in the CP-grid simulation. Simulations with second-order and fourth-order diffusion terms in the thermodynamic equation show that the diffusion modifies the large-scale flow also in the L-grid simulation, indicating nonlinear interactions with the spuriously growing short waves.

In the design of the new finite-difference schemes for the primitive equations based on the CP grid, we have used a generalized σ coordinate. There are advantages, however, when using an isentropic coordinate away from the surface. We have completed the design of a vertically discrete model based on a generalized vertical coordinate that can be basically a σ coordinate near the surface and an isentropic coordinate away from the surface, with a gradual transition between the two.

Acknowledgments. The authors wish to thank Dr. Carlos R. Mechoso for his support and encouragement and Drs. David Burridge and Andrew Staniforth for their useful suggestions and comments on the original manuscript. This research is funded under NSF ATM-9224863 and -9114850, NASA NAG5-2591, and DOE-CHAMMP-DE-FG03-91ER61214. Computations are performed at computer facilities at NCAR and UCLA Department of Atmospheric Sciences.

APPENDIX A

A Summary of the System of Discrete Equations Based on the Generalized σ Coordinate, $\sigma = F(p, p_S)$

Continuity equation

$$\frac{\partial m_l}{\partial t} + \nabla\cdot(m\mathbf{v})_l + \frac{1}{(\delta\sigma)_l}[(m\dot\sigma)_{l+1/2} - (m\dot\sigma)_{l-1/2}] = 0 \quad \text{for } l = 1, 2, \cdots, L, \quad \text{(A.1)}$$

where $m_l \equiv (p_{l+1/2} - p_{l-1/2})(\delta\sigma)_l^{-1}$ and $(\delta\sigma)_l \equiv \sigma_{l+1/2} - \sigma_{l-1/2}$.

Boundary conditions

$$(m\dot\sigma)_{1/2} = (m\dot\sigma)_{L+1/2} = 0. \quad \text{(A.2)}$$

Thermodynamic energy equation

$$\frac{\partial}{\partial t} m_{l+1/2}c_pT_{l+1/2} + \nabla\cdot[(m\mathbf{v})_{l+1/2}c_pT_{l+1/2}] + \frac{c_p}{(\delta\sigma)_{l+1/2}}[(Tm\dot\sigma)_{l+1} - (Tm\dot\sigma)_l] = (m\alpha\omega)_{l+1/2} + (mQ)_{l+1/2} \quad \text{for } l = 1, 2, \cdots, L-1, \quad \text{(A.3)}$$

where

$$(m\mathbf{v})_{l+1/2} \equiv \frac{1}{2(\delta\sigma)_{l+1/2}}[(\delta\sigma)_l(m\mathbf{v})_l + (\delta\sigma)_{l+1}(m\mathbf{v})_{l+1}] \quad \text{for } l = 1, 2, \cdots, L-1. \quad \text{(A.4)}$$

Here $(\delta\sigma)_{l+1/2} = 0.5[(\delta\sigma)_l + (\delta\sigma)_{l+1}]$. In (A.3),

$$(Tm\dot\sigma)_l \equiv \frac{1}{2}[T_{l-1/2}(m\dot\sigma)_{l+1/2} + T_{l+1/2}(m\dot\sigma)_{l-1/2}] \quad \text{for } l = 1, 2, \cdots, L, \quad \text{(A.5)}$$

and

$$(m\alpha\omega)_{l+1/2} \equiv \frac{RT_{l+1/2}}{p_{l+1/2}}\Big[-m_{l+1/2} \times \sum_{k=1}^{l}\nabla\cdot(m_k\mathbf{v}_k)(\delta\sigma)_k + (m\mathbf{v})_{l+1/2}\cdot\nabla p_{l+1/2}\Big] \quad \text{for } l = 1, 2, \cdots, L-1. \quad \text{(A.6)}$$

At the upper and lower boundaries,

$$\frac{\partial}{\partial t} m_1c_pT_{1/2} + \nabla\cdot[(m\mathbf{v})_1c_pT_{1/2}] + \frac{c_pT_{1/2}}{(\delta\sigma)_1}(m\dot\sigma)_{3/2} = (mQ)_{1/2} \quad \text{(A.7)}$$

and

$$\frac{\partial}{\partial t} m_lc_pT_{L+1/2} + \nabla\cdot[(m\mathbf{v})_Lc_pT_{L+1/2}] - \frac{c_pT_{L+1/2}}{(\delta\sigma)_L}(m\dot\sigma)_{L-1/2} = (m\alpha\omega)_{L+1/2} + (mQ)_{L+1/2}, \quad \text{(A.8)}$$

respectively. In (A.8),

$$(m\alpha\omega)_{L+1/2} \equiv \frac{RT_{L+1/2}}{p_{L+1/2}}\Big[-m_L\sum_{k=1}^{L}\nabla\cdot(m\mathbf{v})_k(\delta\sigma)_k + (m\mathbf{v})_L\cdot\nabla p_{L+1/2}\Big]. \quad \text{(A.9)}$$

Hydrostatic equation

$$\Phi_l - \Phi_{l+1} = \frac{(p_{l+3/2} - p_{l-1/2})RT_{l+1/2}}{2p_{l+1/2}},$$

$$\text{for} \quad l = 1, 2, \cdots, L-1. \quad \text{(A.10)}$$

At the lower boundary,

$$\Phi_L - \Phi_{L+1/2} = \frac{(p_{L+1/2} - p_{L-1/2})RT_{L+1/2}}{2p_{L+1/2}}. \quad \text{(A.11)}$$

Vertical mass flux

$$-\left(\frac{\partial F}{\partial p}\right)_{l+1/2}(m\dot{\sigma})_{l+1/2} = \left(\frac{\partial F}{\partial p}\right)_{l+1/2}\sum_{k=1}^{l}\nabla\cdot(m\mathbf{v})_k(\delta\sigma)_k + \left(\frac{\partial F}{\partial p_S}\right)_{l+1/2}\sum_{k=1}^{L}\nabla\cdot(m\mathbf{v})_k(\delta\sigma)_k$$

$$\text{for} \quad l = 1, 2, \cdots, L-1, \quad \text{(A.12)}$$

where $\sigma_{l+1/2} \equiv F(p_{l+1/2}, p_S)$. At the upper and lower boundaries,

$$(m\dot{\sigma})_{1/2} = (m\dot{\sigma})_{L+1/2} = 0. \quad \text{(A.13)}$$

Horizontal pressure gradient force

$$-(\nabla_p\Phi)_l = -\frac{1}{m_l}\nabla(m_l\Phi_l) - \frac{1}{m_l(\delta\sigma)_l}[\Phi_{l+1/2}\nabla p_{l+1/2} - \Phi_{l-1/2}\nabla p_{l-1/2}]$$

$$\text{for} \quad l = 1, 2, \cdots, L. \quad \text{(A.14)}$$

APPENDIX B

A Linear Model for Horizontally Standing Waves

a. Governing equations

We consider the following linearized equations in a p coordinate for meridionally uniform perturbations on a resting isothermal basic state on a zonally cyclic f plane:

$$\frac{\partial u'}{\partial t} = -\frac{\partial \Phi'}{\partial x} + fv', \quad \text{(B.1)}$$

$$\frac{\partial v'}{\partial t} = -fu', \quad \text{(B.2)}$$

$$\frac{\partial \theta'}{\partial t} + \omega'\frac{\partial \bar{\theta}}{\partial p} = -\lambda(\theta' - \theta^{*\prime}), \quad \text{(B.3)}$$

$$\frac{\partial u'}{\partial x} + \frac{\partial \omega'}{\partial p} = 0, \quad \text{(B.4)}$$

$$\frac{\partial \Phi'}{\partial p} = -\frac{\partial \Pi}{\partial p}\theta', \quad \text{(B.5)}$$

where θ^* is an equilibrium value of θ, which may vary in x as well as in p, λ is a constant relaxation coefficient, and the overbar represents the basic state. At the upper and bottom boundaries,

$$\omega' = 0 \quad \text{(B.6)}$$

and

$$w' = 0, \quad \text{(B.7)}$$

respectively, when w is the vertical velocity. The bottom boundary condition (B.7) yields

$$\frac{\partial \Phi_S'}{\partial t} + \left(\omega'\frac{\partial \bar{\Phi}}{\partial p}\right)_S = 0, \quad \text{(B.8)}$$

where the subscript S denotes the lower boundary. For the resting basic state,

$$\frac{\partial \bar{\Phi}}{\partial p} = -\frac{\partial \Pi}{\partial p}\bar{\theta}. \quad \text{(B.9)}$$

We assume that the perturbations are in the following forms: $u'(x, p, t) \equiv \hat{u}(p, t)\cos kx$, $v'(x, p, t) \equiv \hat{v}(p, t)\cos kx$, $\theta'(x, p, t) \equiv \hat{\theta}(p, t)\sin kx$, $\theta^{*\prime}(x, p) \equiv \hat{\theta}^*(p)\sin kx$, $\Phi'(x, p, t) \equiv \hat{\Phi}(p, t)\sin kx$, $\omega'(x, p, t) \equiv \hat{\omega}(p, t)\sin kx$, and $\Phi_S'(x, t) \equiv \hat{\Phi}_S(t)\sin kx$, where k is the zonal wavenumber.

b. Vertically discrete equations in the L grid

Equations (B.1)–(B.9) can be discretized on the L-grid using $u_l'(x, t) \equiv \hat{u}_l(t)\cos kx$, $v_l'(x, t) \equiv \hat{v}_l(t)\cos kx$, $\theta_l'(x, t) \equiv \hat{\theta}_l(t)\sin kx$, $\theta_l^{*\prime}(x) \equiv \hat{\theta}_l^*\sin kx$, $\Phi_l'(x, t) \equiv \hat{\Phi}_l(t)\sin kx$, $\omega_{l+1/2}'(x, t) \equiv \hat{\omega}_{l+1/2}(t)\sin kx$, and $\Phi_{L+1/2}'(x, t) \equiv \hat{\Phi}_{L+1/2}(t)\sin kx$ as

$$\frac{d\hat{u}_l}{dt} = -k\hat{\Phi}_l + f\hat{v}_l \quad \text{for} \quad l = 1, 2, \cdots, L, \quad \text{(B.10)}$$

$$\frac{d\hat{v}_l}{dt} = -f\hat{u}_l \quad \text{for} \quad l = 1, 2, \cdots, L, \quad \text{(B.11)}$$

$$\frac{d\hat{\theta}_l}{dt} = -\frac{1}{2}\left[\left(\frac{\partial \bar{\theta}}{\partial p}\right)_{l+1/2}\hat{\omega}_{l+1/2} + \left(\frac{\partial \bar{\theta}}{\partial p}\right)_{l-1/2}\hat{\omega}_{l-1/2}\right] - \lambda(\hat{\theta}_l - \hat{\theta}_l^*) \quad \text{for} \quad l = 1, 2, \cdots, L, \quad \text{(B.12)}$$

$$\hat{\omega}_{l+1/2} = \hat{\omega}_{l-1/2} + k\hat{u}_l(\delta p)_l \quad \text{for} \quad l = 1, 2, \cdots, L, \quad \text{(B.13)}$$

$$\hat{\Phi}_l = \hat{\Phi}_{l+1} + \left(\frac{\partial \Pi}{\partial p}\right)_{l+1/2}\left(\frac{\hat{\theta}_{l+1} + \hat{\theta}_l}{2}\right)(\delta p)_{l+1/2} \quad \text{for} \quad l = 1, 2, \cdots, L-1, \quad \text{(B.14)}$$

$$\hat{\Phi}_L = \hat{\Phi}_{L+1/2} + \left(\frac{\partial \Pi}{\partial p}\right)_{L+1/2} \hat{\theta}_L \frac{(\delta p)_L}{2}. \quad \text{(B.15)}$$

At the upper and lower boundaries,

$$\hat{\omega}_{1/2} = 0 \quad \text{(B.16)}$$

and

$$\frac{d\hat{\Phi}_{L+1/2}}{dt} = -\left(\frac{\partial \bar{\Phi}}{\partial p}\right)_{L+1/2} \hat{\omega}_{L+1/2}, \quad \text{(B.17)}$$

respectively. In (B.10)–(B.17), $(\delta p)_l \equiv p_{l+1/2} - p_{l-1/2}$ and $(\delta p)_{l+1/2} \equiv 0.5[(\delta p)_{l+1} + (\delta p)_l]$. In the integrations, we use $(\partial \bar{\theta}/\partial p)_{l+1/2} \equiv -RT_0(\Pi p)^{-1}_{l+1/2}$ and $(\partial \bar{\Phi}/\partial p)_{L+1/2} \equiv -RT_0/p_{L+1/2}$, where T_0 is the temperature of the basic isothermal state. The vertical grid is equally spaced in $\zeta_{l+1/2} = \ln(p_{l+1/2}/p_0)$. Under these conditions for the L grid, Arakawa and Lamb (1977) show that there is no internal reflections when $\lambda = 0$.

c. *Discrete equations on the CP grid*

Similar to the case of the L grid but using $\theta'_{l+1/2}(x, t) \equiv \hat{\theta}_{l+1/2}(t) \sin kx$ and $\theta^{*\prime}_{l+1/2}(x) \equiv \hat{\theta}^*_{l+1/2} \sin kx$, we write

$$\frac{d\hat{u}_l}{dt} = -k\hat{\Phi}_l + f\hat{v}_l \quad \text{for} \quad l = 1, 2, \cdots, L, \quad \text{(B.18)}$$

$$\frac{d\hat{v}_l}{dt} = -f\hat{u}_l \quad \text{for} \quad l = 1, 2, \cdots, L, \quad \text{(B.19)}$$

$$\frac{d\hat{\theta}_{l+1/2}}{dt} = -\left(\frac{\partial \bar{\theta}}{\partial p}\right)_{l+1/2} \hat{\omega}_{l+1/2} - \lambda(\hat{\theta}_{l+1/2} - \hat{\theta}^*_{l+1/2})$$

$$\text{for} \quad l = 0, 1, \cdots, L, \quad \text{(B.20)}$$

$$\hat{\omega}_{l+1/2} = \hat{\omega}_{l-1/2} + k\hat{u}_l(\delta p)_l \quad \text{for} \quad l = 1, 2, \cdots, L, \quad \text{(B.21)}$$

$$\hat{\Phi}_l = \hat{\Phi}_{l+1} + \left(\frac{\partial \Pi}{\partial p}\right)_{l+1/2} \hat{\theta}_{l+1/2}(\delta p)_{l+1/2}$$

$$\text{for} \quad l = 1, 2, \cdots, L-1, \quad \text{(B.22)}$$

$$\hat{\Phi}_L = \hat{\Phi}_{L+1/2} + \left(\frac{\partial \Pi}{\partial p}\right)_{L+1/2} \hat{\theta}_{L+1/2} \frac{(\delta p)_L}{2}. \quad \text{(B.23)}$$

At the upper and lower boundaries

$$\hat{\omega}_{1/2} = 0 \quad \text{(B.24)}$$

and

$$\frac{d\hat{\Phi}_{L+1/2}}{dt} = -\left(\frac{\partial \bar{\Phi}}{\partial p}\right)_{L+1/2} \hat{\omega}_{L+1/2}, \quad \text{(B.25)}$$

respectively. In (B.18)–(B.25), $(\delta p)_l \equiv p_{l+1/2} - p_{l-1/2}$ and $(\delta p)_{l+1/2} \equiv 0.5[(\delta p)_{l+1} + (\delta p)_l]$. In the integrations we use $(\partial \bar{\theta}/\partial p)_{l+1/2} \equiv -RT_0(\Pi p)^{-1}_{l+1/2}$ and $(\partial \bar{\Phi}/\partial p)_{L+1/2} \equiv -RT_0/p_{L+1/2}$. The vertical grid is equally spaced in $\zeta_{l+1/2} = \ln(p_{l+1/2}/p_0)$.

If we assume that the time-dependent part of the solution has the form $\exp(-i\nu t)$, where ν is the frequency, we obtain a discrete vertical structure equation away from the vertical boundaries as

$$\frac{\hat{W}_{l+3/2} - 2\hat{W}_{l+1/2} + \hat{W}_{l-1/2}}{(\delta\zeta)^2} + \tilde{n}^2\hat{W}_{l+1/2} = 0, \quad \text{(B.26)}$$

where $\lambda = 0$ is assumed, and we used $\hat{W}_{l+1/2} \equiv p^{-1/2}_{l+1/2} \times \hat{\omega}_{l+1/2}$, $p_l \equiv (p_{l+1/2}p_{l-1/2})^{1/2}$ and

$$\tilde{n}^2 \equiv \frac{k^2 S_{l+1/2} p^2_{l+1/2}}{f^2 - \nu^2} e^{(\delta\zeta)/2} + \frac{1 - e^{(\delta\zeta)}}{(\delta\zeta)^2}. \quad \text{(B.27)}$$

For an isothermal atmosphere, $S_{l+1/2}p^2_{l+1/2}$, where $S_{l+1/2} \equiv [(\partial\Pi/\partial p)(\partial\bar{\theta}/\partial p)]_{l+1/2}$ and, therefore, $\tilde{n}^2$ are constants.

REFERENCES

Arakawa, A., 1972: Design of the UCLA general circulation model. Numerical Simulation of Weather and Climate, Tech. Rep. 7, Department of Meteorology, University of California, Los Angeles, Los Angeles, CA, 116 pp.

——, 1988: Finite-difference methods in climate modeling. *Physically-Based Modelling and Simulation of Climate and Climatic Change,* Part I, M. E. Schlesinger, Ed., Kluwer, 79–168.

——, and V. Lamb, 1977: Computational design of the basic dynamical processes of the UCLA general circulation model. *Methods in Computational Physics,* Vol. 17, J. Chang, Ed., Academic Press, 173–265.

——, and M. J. Suarez, 1983: Vertical differencing of the primitive equations in sigma coordinates. *Mon. Wea. Rev.,* **111,** 34–45.

——, and S. Moorthi, 1988: Baroclinic instability in vertically discrete systems. *J. Atmos. Sci.,* **45,** 1688–1707.

——, and Y.-J. G. Hsu, 1990: Energy conserving and potential-enstrophy dissipating schemes for the shallow water equations. *Mon. Wea. Rev.,* **118,** 1960–1969.

Bourke, W., 1974: A multi-level spectral model. Part I: Formulation and hemispheric integrations. *Mon. Wea. Rev.,* **102,** 687–701.

Charney, J. G., and N. A. Phillips, 1953: Numerical integration of the quasigeostrophic equations for barotropic and simple baroclinic flows. *J. Meteor.,* **10,** 71–99.

Cullen, M. J. P., and J. James, 1994: A comparison of two different vertical grid staggerings. Preprints, *10th Conf. on Numerical Weather Prediction,* Portland, OR, Amer. Meteor. Soc., 38–40.

Hollingsworth, A., 1995: A spurious mode in the "Lorenz" arrangement of Φ and T which does not exist in the "Charney–Phillips" arrangement. ECMWF Tech. Memo. No. 211, 12 pp.

Hsu, Y.-J. G., and A. Arakawa, 1990: Numerical modeling of the atmosphere with an isentropic vertical coordinate. *Mon. Wea. Rev.,* **118,** 1933–1959.

Krishnamurti, T. N., 1969: An experiment in numerical prediction in equatorial latitudes. *Quart. J. Roy. Meteor. Soc.,* **95,** 594–620.

Lorenz, E. N., 1960: Energy and numerical weather prediction. *Tellus,* **12,** 364–373.

Phillips, N. A., 1957: A coordinate system having some special advantages for numerical forecasting. *J. Meteor.,* **14,** 184–185.

Robert, A. J., J. Henderson, and C. Turnbull, 1972: An implicit time integration scheme for baroclinic models of the atmosphere. *Mon. Wea. Rev.,* **100,** 329–335.

Simmons, A. J., and M. Burridge, 1981: An energy and angular-momentum conserving vertical finite-difference scheme and hybrid vertical coordinates. *Mon. Wea. Rev.,* **109,** 758–766.

Tokioka, T., 1978: Some consideration on vertical differencing. *J. Meteor. Soc. Japan,* **56,** 89–111.